Monatshefte für Chemie 133, 1555–1574 (2002)
DOI 10.1007/s00706-002-0519-2

Monatshefte für Chemie
Chemical Monthly
Printed in Austria

The Flexibility of SIMPSON and SIMMOL for Numerical Simulations in Solid- and Liquid-State NMR Spectroscopy

Thomas Vosegaard*, **Anders Malmendal,** and **Niels C. Nielsen***

Interdisciplinary Nanoscience Center (iNANO) and Laboratory for Biomolecular NMR Spectroscopy, Department of Molecular and Structural Biology, University of Aarhus, DK-8000 Aarhus C, Denmark

Received June 27, 2002; accepted July 8, 2002
Published online November 7, 2002

Summary. Addressing the need for numerical simulations in the design and interpretation of advanced solid- and liquid-state NMR experiments, we present a number of novel features for numerical simulations based on the SIMPSON and SIMMOL open source software packages. Major attention is devoted to the flexibility of these Tcl-interfaced programs for numerical simulation of NMR experiments being complicated by demands for efficient powder averaging, large spin systems, and multiple-pulse rf irradiation. These features are exemplified by fast simulation of second-order quadrupolar powder patterns using crystallite interpolation, analysis of rotary resonance triple-quantum excitation for quadrupolar nuclei, iterative fitting of MQ-MAS spectra by combination of SIMPSON and MINUIT, simulation of multiple-dimensional PISEMA-type correlation experiments for macroscopically oriented membrane proteins, simulation of *Hartman-Hahn* polarization transfers in liquid-state NMR, and visualization of the spin evolution under complex composite broad-band excitation pulses.

Keywords. Solid-state NMR; Numerical simulations; Software; Membrane proteins; Inorganic materials.

Introduction

Over the past decades NMR spectroscopy has evolved tremendously by the development of powerful instrumentation and the design of thousands of advanced NMR experiments [1–3] offering almost complete control over the nuclear spin Hamiltonian to extract detailed information about the structure and dynamics of large molecules. This development has been facilitated by the use of theoretical tools such as average Hamiltonian theory [4–6] and the product operator formalism [7–9]. These tools have proved extremely useful for description of the spin

* Corresponding authors. E-mail: tv@chem.au.dk, ncn@imsb.au.dk

dynamics in relatively small spin systems subjected to well-defined rotations in pulsed experiments with a reasonable small number of distinct time events.

Parallel to the development of increasingly complex NMR experiments capable of handling more and more complex nuclear spin systems comes an increasing need for tools to accurately evaluate the performance of these experiments with the purpose of further development, artifact suppression, or interpretation of experimental data. This applies in particular for large spin systems, in presence of anisotropic nuclear spin interactions, and under conditions of imperfect rf irradiation. Solid-state NMR spectroscopy [10–14] very often faces all of these elements. Anisotropic nuclear spin interactions [11] introduce orientation dependent spin evolution which often is sufficiently strong that it not only affects free precession but also causes anisotropic evolution in periods with rf irradiation. In addition to this may come effects from ultra-fast sample spinning. Very often the experiments rely on delicate tailoring of the nuclear spin Hamiltonian by synchronous sample rotation and multiple-pulse rf irradiation to selectively re- and decouple specific interactions [15–27]. For example, methods of this kind have formed an indispensable basis for the current implementation of multiple-dimensional solid-state NMR for structural analysis of uniformly ^{13}C and ^{15}N labeled proteins immobilized by size, aggregation, or membrane association [28, 29].

To provide the spin engineers and application-oriented spectroscopists using NMR for structural analysis with tools for efficient numerical simulation of advanced solid- and liquid-state NMR experiments, we recently introduced the SIMPSON [30] and SIMMOL [31] programs as open source software. SIMPSON is a highly flexible program package for easy programming and simulation of essentially all types of solid-state NMR experiments. The amount and complexity of programming is very modest and similar to that required for implementation of pulse sequences on a commercial NMR spectrometers. As so this package may be considered a ''computer spectrometer''. To facilitate the setup of spin systems and in particular anisotropic interaction tensors for SIMPSON simulations, we recently introduced the SIMMOL program (and its predecessor PDB2SIMPSON [32]) to serve as a ''sample-changer'' for the ''computer spectrometer''. As an additional benefit, these programs enable straightforward visualization of relevant parts of the molecular structure with specification of relevant anisotropic NMR interactions.

Results and Discussion

While our previous accounts [30–32] have primarily described SIMPSON and SIMMOL individually as specific tools for solid-state NMR simulations, we will in this paper focus more on the flexibility of the two tools and their combination for numerical simulations in a broad spectrum of applications within solid- and liquid-state NMR spectroscopy. The key to this flexibility is the Tcl [33] scripting interfaces of SIMPSON and SIMMOL which offer unique possibilities for their control, mutual interaction, and even interaction with other programs through simple Tcl commands. These features will be demonstrated by (*i*) fast simulations of second-order quadrupolar powder patterns under magic-angle spinning (MAS) employing crystallite interpolation, (*ii*) fast simulation of triple-quantum (3Q) coherence excitation in quadrupolar nuclei using rotary resonance, (*iii*) fitting of experimental

solid-state NMR spectra using SIMPSON in combination with MINUIT [34], (*iv*) SIMPSON and SIMMOL simulations of multi-dimensional PISEMA-type experiments for the study of macroscopically oriented membrane proteins, (*v*) optimization of *Hartman-Hahn* polarization transfer experiments in liquid-state NMR [3], and (*vi*) visualization of the spin evolution during complex hypersecant composite pulses. Overall these examples not only serve to demonstrate the flexibility of SIMPSON and SIMMOL but also represent important new extensions of these programs for advanced applications through development of routines for time-efficient calculations of complex state-of-the-art NMR experiments [35].

SIMPSON Flexibility: Fast Simulation of Second-Order Quadrupolar Powder Patterns by Crystallite Interpolation

Most of the nuclear spin interactions are orientation dependent. In solid-state NMR of poly-crystalline samples (and other samples with no orientational preference), the anisotropic interactions typically result in broad powder patterns because different orientations of the ''crystallites'' relative to the external magnetic field will be associated with different resonance frequencies [11, 14]. In such cases a simulated spectrum is achieved by integration over all possible crystallite orientations (i) each of which being characterized by three *Euler* angles ($\alpha_i, \beta_i, \gamma_i$) describing the orientation of the crystallite relative to the magnetic field. Since there are generally no analytical solutions to the integral, a standard procedure is to calculate the sum of the spectra for different crystallite orientations, weighted by the space angle spanned by the particular crystallite (w_i). Among the three *Euler* angles the γ-angle is special. For static powders the spectra are independent on γ, since the NMR interactions are invariant to rotation about the stationary field. For rotating solids, γ may be parametrized simultaneously with the sample rotation angle [36–40]. The α, β crystallites may be established randomly (Monte Carlo type), by rectangular or spherical grids, or more efficiently using tiling schemes with more uniform crystallite weight factors such as *Zaremba-Conroy-Wolfsberg* [41–43], SOPHE [44], *Alderman* [45], REPULSION [46], or Gaussian spherical quadrature [47] methods. While a relatively small set of well-defined *Euler* angles suffices for simulation of narrow powder patterns or spinning-sideband manifolds of such line shapes as being typical for MAS experiments of spin-$1/2$ nuclei, it is well-known that very broad powder patterns as often encountered for quadrupolar nuclei may require a much larger number of crystallite orientations in a carefully chosen tiling scheme.

Addressing exactly this problem, *Alderman et al.* [45] proposed an interpolation procedure that significantly reduces the number of crystallites needed to achieve a converged line shape. In this approach the resonance frequencies are first calculated for a relatively coarse set of α, β crystallites as represented by vertexes between the dark lines on the unit sphere in Fig. 1a. Next the resonance frequencies defining the vertexes of each triangle on the unit sphere (*e.g.*, the three crystallites labeled i, j, and k in Fig. 1a) are sorted as $\nu_{\min}$, ν_{mid}, and $\nu_{\max}$, representing the lowest, middle, and highest frequency, respectively. It is assumed that all crystallites within the space angle spanned by the triangle give resonance frequencies within the frequency range [$\nu_{\min}$, $\nu_{\max}$], and that the frequency spectrum

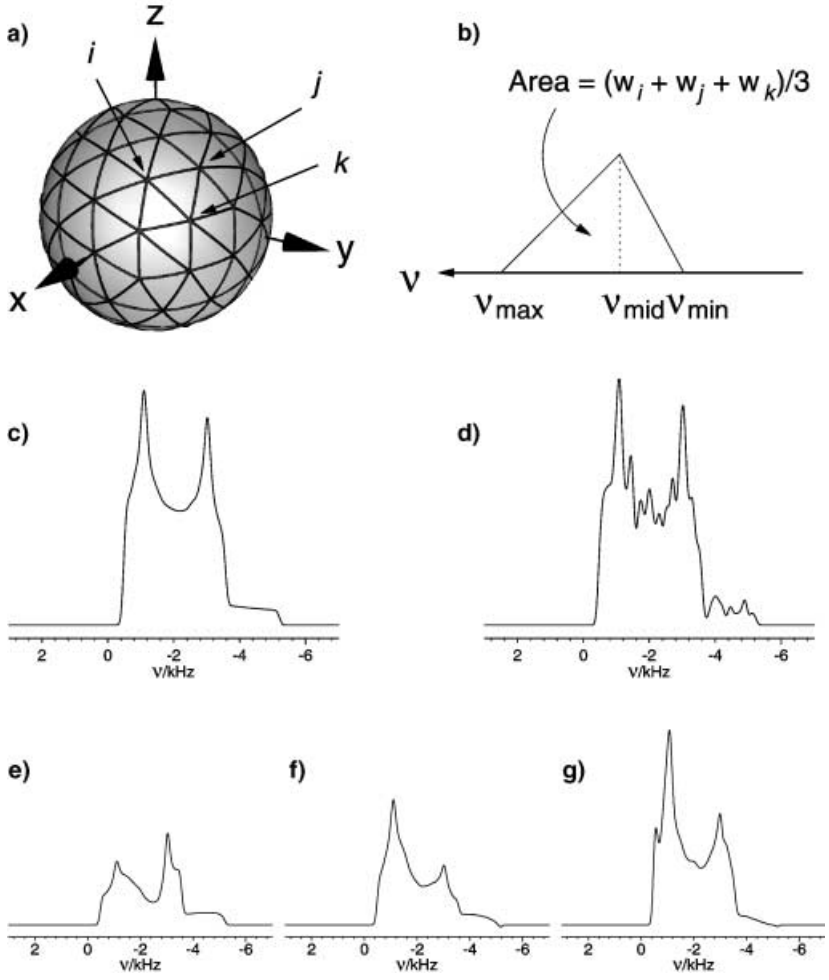

Fig. 1. Crystallite distribution of 100 REPULSION crystallites over the unit sphere. The crystallites labeled *i*, *j*, and *k* are located at the vertexes of a triangle. (b) Triangle corresponding to the spectrum from (α, β) points within the triangle defined by the crystallites *i*, *j*, and *k*. $\nu_{\min}$, ν_{mid}, and $\nu_{\max}$ represent the lowest, middle, and highest resonance frequencies of the three vertexes. (c, d) Simulated 9.4-T ^{87}Rb powder spectra of $RbClO_4$ assuming ideal rf excitation, quadrupole coupling parameters of $C_Q = 3.3$ MHz and $\eta_Q = 0.21$ [50, 51], resulting from interpolation with 625 *Alderman* crystallites (c) and 678 REPULSION crystallites without interpolation (d). (e–g) Simulated 3Q-filtered MAS spectra with the same quadrupole coupling parameters and employing short-pulse (e), RIACT (f), and FASTER (g) 3Q excitation using the parameters in Table 1. All simulations (c–g) employ $\omega_r/2\pi = 30$ kHz and are apodized by a Gaussian line broadening of 150 Hz

for the triangle may be represented by a triangle ranging from $\nu_{\min}$ to $\nu_{\max}$ with maximum intensity at ν_{mid} as illustrated in Fig. 1b. The area of this triangle corresponds to the space angle of the crystallite triangle [45].

This interpolation method requires that the simulation can be performed directly in the frequency domain and that each crystallite gives a well-defined resonance frequency or set of such frequencies. This generally applies for static samples when the Hamiltonian is diagonal. For quadrupolar nuclei in MAS

experiments, the second-order line shape is, to a good approximation, determined by a static component [48] depending only on the α and β angles (*vide infra*). Since γ and $\omega_r t$ both correspond to rotation around the rotor axis and the γ angle may distribute the intensity of the crystallite over the entire manifold of second-order quadrupolar spinning sidebands, this case is typically referred to as the infinite spinning frequency approximation. Although beyond the scope of this example, we note that interpolation-based powder averaging may also be constructed for more general cases with finite sample spinning [49] being particularly easy in the case of diagonal Hamiltonians [37]. In the typical case where the spectrum is excited using finite rf pulses, the orientation dependent intensity distribution may be included in the powder averaging by adjusting the weighting factor (w_i) for crystallite i to $w_i \rightarrow w_i \rho_i$, where ρ_i is the density operator element of interest for crystallite i at the beginning of the acquisition.

With the relevance of interpolation, in particular in presence of an orientation-dependent excitation profile, it is most relevant to address how this efficiently can be implemented into SIMPSON exploiting the flexibility of the Tcl interface. For the purpose of illustration, we consider the simulation of second-order quadrupolar powder patterns as achieved in the very popular multiple-quantum magic-angle spinning (MQ-MAS) experiments proposed by *Frydman* and co-workers [52, 53] for acquiring isotropic spectra of quadrupolar nuclei. This experiment relies on excitation of triple-quantum (3Q) coherences and mixing of these into detectable single-quantum coherences. Both of these processes are generally associated with rather low transfer amplitudes depending on the magnitude and orientation of the quadrupolar interaction tensor. For this reason the second-order quadrupolar powder pattern may be highly distorted by different excitation efficiencies for different crystallites. Such cases typically call for numerical simulations as demonstrated here by SIMPSON calculation of the 3Q excitation profile in MAS experiments. We note that the infinite spinning approximation may be justified in these examples since spinning sidebands are virtually non-existing in 3Q-filtered MAS experiments [54].

The resonance frequency for a single-quantum $(m, m-1)$ transition influenced by the second-order quadrupolar Hamiltonian ($\mathcal{H}_Q^{(2)}$) may be written

$$\begin{aligned}\omega_m(\alpha,\beta,\gamma;t) &= \langle m|\mathcal{H}_Q^{(2)}(\alpha,\beta,\gamma;t)|m\rangle - \langle m-1|\mathcal{H}_Q^{(2)}(\alpha,\beta,\gamma;t)|m-1\rangle \\ &= \sum_{l=-4}^{4} \omega_{m,m-1}^{l}(\alpha,\beta)\exp\{-il(\omega_R t+\gamma)\} \qquad (1)\end{aligned}$$

where the time-independent $l=0$ term governs the second-order line shape and $\omega_{m,m-1}^{0}$ is the resonance frequency for the α,β crystallite. The $l\neq 0$ terms are thereby responsible for the second-order quadrupolar spinning sidebands and are not relevant when operating in the infinite spinning rate approximation. We may isolate the $l=0$ term by averaging the resonance frequency over 2^n $(n\geq 3)$ γ crystallites which cancels all the oscillating terms.

In SIMPSON the Hamiltonian and density matrices are evaluated and stored in the memory during the calculation. These matrices may be accessed in the Tcl interface by the SIMPSON supplied commands `matrix get hamiltonian` and `matrix get density`. In a standard calculation of the solid-state NMR

spectrum we will pick out the density operator element corresponding to I_- for the central $\left(\frac{1}{2}, -\frac{1}{2}\right)$ transition (specified by the single-transition I_-^{2-3} operator for a spin-3/2 nucleus) and calculate the corresponding resonance frequency as described in Eq. (1). However, as we in this case merely want to investigate the impact of imperfect *excitation* (*i.e.*, assuming ideal $3Q \rightarrow 1Q$ mixing) we will instead evaluate the density operator element corresponding to 3Q coherence (I_+^{1-4}) after the excitation. Once we know the density operator element and the resonance frequency for each set of crystallite *Euler* angles (α_i, β_i), the triangular interpolation may be performed as described above. It should be noted that this approach provides the exact spinning-frequency dependent excitation profile while the infinite spinning rate approximation is only used during the acquisition.

We have written a Tcl procedure to add the triangles to a spectrum (identified by the spectrum descriptor `$f`) as

```
faddtriangle $f $freq_i $freq_j $freq_k $w_re $w_im
```

which takes as input the resonance frequencies at the three vertexes (*i*, *j*, and *k*) in addition to the real and imaginary weighting factors for the triangle. The latter factors are calculated by Eqs. (2) and (3).

$$\texttt{w\_re} = (w_i \mathrm{Re}(\rho_i) + w_j \mathrm{Re}(\rho_j) + w_k \mathrm{Re}(\rho_k))/3, \tag{2}$$

$$\texttt{w\_im} = (w_i \mathrm{Im}(\rho_i) + w_j \mathrm{Im}(\rho_j) + w_k \mathrm{Im}(\rho_k))/3. \tag{3}$$

A first illustration of the advantage of using crystallite interpolation is given in Figs. 1c and 1d showing ideal (no effects from non-uniform excitation) second-order quadrupolar powder patterns for a ^{87}Rb nucleus with the quadrupole coupling parameters of $RbClO_4$ [50, 51] resulting from interpolation of 625 *Alderman* crystallites (Fig. 1c) and 678 REPULSION crystallites without interpolation (Fig. 1c). It is apparent from these spectra that far more crystallites are needed to achieve convergence of the line shape without interpolation, and that the result from the interpolation closely resembles an ideal second-order quadrupolar line shape. Different basis crystallite sets were used for the two simulations since we have observed that the uniformly distributed REPULSION crystallites typically provide better line shapes than *Alderman* crystallites when no interpolation is used, while the *Alderman* crystallites appear to be slightly better suited for interpolation.

Numerous techniques employing hard pulses [53], composite pulses [55], shaped pulses [56], rotation-induced adiabatic coherence transfer (RIACT) [57], fast amplitude-modulation [58–60], double frequency sweeps [61], and rotary-resonance (FASTER) [27] excitation have been presented in order to ameliorate the relatively low excitation and mixing efficiency and thereby sensitivity of the MQ-MAS experiment. We note that the sensitivity may additionally be improved by up to an order of magnitude in the detection part of the experiment by sampling through a train of QCPMG pulses [62, 63]. In the investigation of the powder patterns resulting from different excitation schemes, we will focus on three techniques, namely short-pulse, RIACT, and FASTER excitation. For each technique, we have performed a numerical search for the optimum parameters for the excitation pulses assuming ^{87}Rb quadrupole coupling parameters of $RbClO_4$ at 9.4 T and spinning at a frequency of 30 kHz. These results are listed in Table 1 and agree well

Table 1. Calculated optimum pulse lengths for the specified rf field strengths used for 3Q excitation with short-pulse, RIACT, and FASTER excitation schemes. The simulations employ $\omega_r/2\pi = 30$ kHz and the ^{87}Rb (spin $I = 3/2$) quadrupole coupling parameters for $RbClO_4$ ($C_Q = 3.3$ MHz, $\eta_Q = 0.21$ [50, 51]) at 9.4 T

Excitation scheme	τ_p/μs	$(\omega_{rf}/2\pi)$/kHz	Relative intensity
Short pulse	4.9	150	1
RIACT[a]	8.3	150	1.26
FASTER	99	37	1.78

[a] The RIACT pulse is preceded by a central-transition selective $\pi/2$ pulse employing an rf field strength of 40 kHz

with typical experimental findings. The simulated spectra obtained using interpolation of 625 *Alderman* crystallites are shown on the same intensity scale in Figs. 1e–1g for short-pulse (e), RIACT (f), and FASTER (g) excitation. Indeed the simulations reflect relative intensities in Table 1. As expected the simulated MQ-MAS line shapes are somewhat distorted compared to the ideal second-order quadrupolar line shape shown in Fig. 1c [63–66].

Overall, we have in this section demonstrated that time-efficient simulation of broad powder spectra using powder averaging in combination with crystallite interpolation may readily be implemented in SIMPSON. This approach has been demonstrated by simulation of second-order quadrupolar line shapes of 3Q filtered MQ-MAS experiments.

Fast Simulations with SIMPSON: Rotary-Resonance Triple-Quantum Excitation for Quadrupolar Nuclei

Analytical and numerical investigations of the effects of finite pulses on quadrupolar nuclei have been performed by numerous groups [27, 63, 67–70]. The prevailing approach has been to divide the calculation into small time increments over each of which the Hamiltonian is assumed to be constant, and evaluate the propagator for each of these fragments for a grid of (α, β, γ) crystallites [68]. As mentioned in the previous section, *Levitt* and *Edén* [36, 39], *Charpentier et al.* [38, 49], and *Hohwy et al.* [40] devised efficient methods for simulation of rotor-synchronous pulse sequences by performing the γ averaging simultaneously with the time incrementation. A comparison of these methods is beyond the scope of this paper, and we focus on the latter, so-called γ-COMPUTE algorithm [40], which is implemented in SIMPSON [30]. We note that γ-COMPUTE may be applied in simulations involving pulse sequences displaying appropriate periodicity with the rotor period [40].

The rotary-resonance [19, 71, 72] based FASTER [27] excitation scheme for MQ-MAS experiments discussed in the previous section reveals that for pulses longer than one rotor period, strong intensity of the 3Q coherence may be achieved when the rf field strength is in-between 3Q coherence zero-crossings at $\omega_{rf} = \omega_r \times n/2$ [27, 73, 74] with n being a positive integer. This effect becomes particularly pronounced at high spinning frequencies. The γ COMPUTE algorithm appears ideal

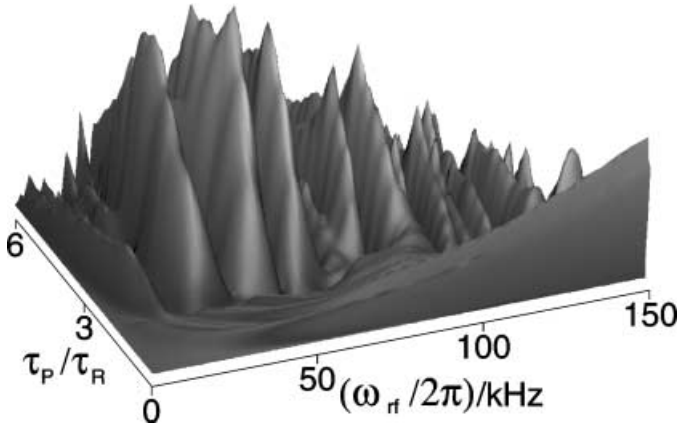

Fig. 2. SIMPSON simulated 3Q intensity as function of pulse length (τ_P) in units of rotor periods and the rf field strength under conditions of $\omega_r/2\pi = 30$ kHz spinning and quadrupole coupling parameters corresponding to ^{87}Rb in $RbClO_4$ [50, 51]

for simulation of this effect since the FASTER excitation sequence simply consists of an rf pulse with constant amplitude applied for several rotor periods.

For the purpose of illustration, we have performed a simulation of the 3Q coherence intensity as function of pulse length and rf field strength as shown in Fig. 2 employing a spinning frequency of 30 kHz and the ^{87}Rb quadrupole coupling parameters of $RbClO_4$ at 9.4 T with 50 time increments per rotor period for 6 rotor periods and rf field strengths from 0 to 150 kHz incremented in steps of 1 kHz. Employing 320 (α, β) REPULSION crystallites (and 50 γ angles) each rf trace was calculated within $\sim$17 s using γ-COMPUTE, while the same result required $\sim$450 s in a direct time-propagation simulation on a 1.9 GHz Pentium IV/Linux workstation. We note that the latter calculation may be speeded up significantly by calculating the propagators only for the first rotor period and subsequently reuse these propagators for the remaining five rotor periods employing the propagator storing facilities in SIMPSON. Using this approach, the calculation of each rf trace lasts $\sim$177 s. In all simulations the time over which the Hamiltonian is assumed to be constant was $1/100$ of a rotor period.

Overall, we demonstrated that time savings in the order of a factor 25 may be achieved using the γ-COMPUTE algorithm instead of direct propagator for simulation of 3Q coherence excitation profiles for FASTER experiments, and a ten-fold time saving as compared to direct propagation with reuse of the propagators. This example shows that although the advantage of γ-COMPUTE is most pronounced for large numbers of points extending over many rotor periods [40], it may still be beneficial to employ this procedure for pulses significantly shorter than one rotor period. In the present example the γ-COMPUTE algorithm remains faster than the direct propagation method for pulse lengths exceeding $\sim 0.2\tau_r$.

SIMPSON Optimization: Combination with MINUIT

To enhance the flexibility of SIMPSON and the capabilities for numerical optimization, we have extended SIMPSON with the minimization tools of the MINUIT

minimization software package from CERN [34]. MINUIT represents a very powerful minimization tool providing options for Monte Carlo optimization, gradient and non-linear minimization, parameter scans, confidence interval calculation, *etc*., while it in full analogy to SIMPSON and SIMMOL is open-source software. In a typical MINUIT minimization, the user has full flexibility to specify the parameters to vary during the minimization, the function to minimize, and the minimization procedure.

SIMPSON may be combined with MINUIT via a Tcl interface alternatingly accessing the two independently compiled programs [75] which demonstrates the great flexibility offered by scripting control. More elegantly, however, we here combine the two programs on the compiled level such that the MINUIT functions may be accessed directly from the SIMPSON Tcl interface. In this setup, the parameters to be optimized may be specified by the command

```
mnpar <name> <value> <error> <min> <max>
```

where the internal name of the parameter, its initial value, the estimated error, and optional minimum and maximum limits are specified. The value of this MINUIT parameter is stored in a Tcl variable `$mn(<name>)` and is thereby accessible from the Tcl interface. The function to minimize is a Tcl procedure `minuit` which returns the value subject to minimization. A typical scenario for determining the isotropic chemical shift and the quadrupolar coupling parameters (C_Q and η_Q) of an experimental spectrum (previously loaded into the descriptor `$g`) could be

```
proc minuit {} {
  global mn g # Make parameters globally available

  set f [fsimpson [list \
    [list shift_1_iso         $mn(iso)] \
    [list quadrupole_1_aniso $mn(cq)]  \
    [list quadrupole_1_eta    $mn(eta)] \
  ]]
  set rms [frms $f $g -re]
  funload $f
  return $rms
}
```

using various standard SIMPSON commands [30]. The minimization procedure is subsequently specified and may involve parameter scans, minimization, fixing and releasing parameters etc. All of these functions are available as SIMPSON Tcl functions, *e.g*., `mnscan`, `mnminimize`, `mnfix`, *etc*., and a typical minimization procedure for the above example could be

```
# Set up parameters
mnpar iso    52     5
mnpar cq      6.8   10
mnpar eta     0.08   0.1   01
```

```
# Minimization procedure
mnscan    iso
mnfix     eta
mnminimize
mnrelease eta
mnminimize
```

which will first perform a linear scan of the isotropic shift, minimize while fixing the quadrupole coupling asymmetry parameter, release it, and do the final minimization of all parameters.

To demonstrate this kind of minimization, we have investigated a previously published [76] ^{27}Al MQ-MAS spectrum of $9Al_2O_3 \cdot 2B_2O_3$ shown in Fig. 3a and recorded at 7.1 T with a spinning frequency of 15 kHz. The trace showing the quadrupolar line shape for the most intense of the Al_V sites is displayed in Fig. 3b. Apart from random noise this trace reveals a quite distorted second-order quadrupolar line shape due to imperfect 3Q excitation and mixing. We will use the interpolation scheme described in the previous section to simulate this spectrum including effects from finite pulses with the experimental values for the pulse lengths ($\tau_{exc} = 3.0\,\mu$s, $\tau_{mix} = 1.4\,\mu$s) and rf field strength ($\omega_{rf}/2\pi = 90$ kHz) [76]. Along with the previously reported quadrupole coupling parameters ($C_Q =$ 6.8 MHz, $\eta_Q = 0.08$, and $\delta_{iso} = 52$ ppm [76]), this should form an excellent starting point for a SIMPSON-MINUIT optimization of the quadrupole coupling parameters from an optimization procedure similar to the one sketched above. The parameters resulting from this optimization are $C_Q = 7.0 \pm 0.2$ MHz, $\eta_Q = 0.11 \pm 0.08$, and $\delta_{iso} = 56 \pm 2$ ppm [35] in good agreement with previously published parameters [76, 77]. The corresponding simulation is shown in Fig. 3c and does indeed reproduce most of the features of the experimental spectrum. For comparison, the

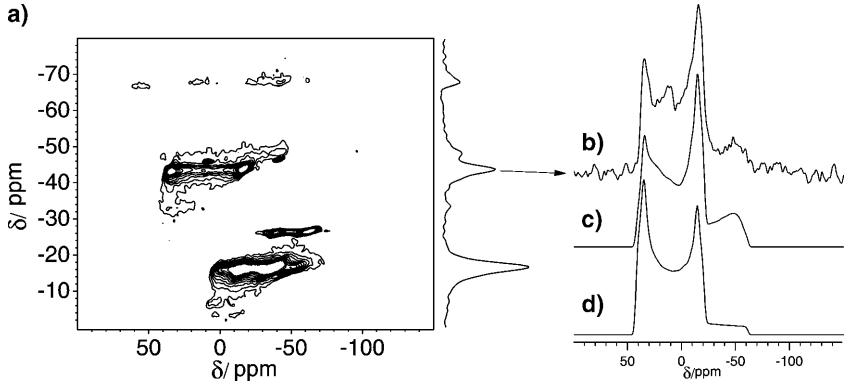

Fig. 3. (a) ^{27}Al MQ-MAS spectrum of $9Al_2O_3 \cdot 2B_2O_3$ recorded at 7.1 T ($\omega_0/2\pi = 78.2$ MHz) using $\omega_r/2\pi = 15$ kHz [76]. The spectrum is obtained using short-pulse excitation and mixing with an rf field strength of 90 kHz and pulse lengths of $\tau_{exc} = 3.0\,\mu$s and $\tau_{mix} = 1.4\,\mu$s. (b) Trace showing the anisotropic line shape for the most intense Al_V site. (c) Simulation including finite-pulse effects and corresponding to the optimum quadrupole coupling parameters ($C_Q = 7.0$ MHz, $\eta_Q = 0.11$, $\delta_{iso} = 56$ ppm). (d) Same simulation but assuming ideal excitation and mixing

simulation resulting from ideal excitation but with identical quadrupole coupling parameters is shown in Fig. 3d. In contrast to the finite-pulse simulation the latter ideal simulation is incapable of modeling the intensity of the experimental spectrum.

To summarize, we have demonstrated that the Tcl controlled SIMPSON and SIMMOL programs can readily be combined with other programs or open source software packages. The specific example addresses the combination of SIMPSON with MINUIT which greatly enhances the capabilities for numerical minimizations for extraction of accurate parameters from experimental NMR spectra or optimization of experimental procedures.

SIMMOL Simulations: Multi-Dimensional PISEMA-Type Experiments for Biological Solid-State NMR

One of the most successful protocols for solid-state NMR studies of membrane proteins, involves macroscopic orientation of the membranes (*e.g.*, phospholipid bilayers) in which the proteins are embedded on glass plates with the membrane normal parallel to the external magnetic field [28]. Since the nuclear spin interactions of the peptide backbone atoms largely possess the same magnitude and orientation relative to the peptide plane, independently on the secondary structure and residue type [31, 78–80], the observed resonance frequencies to a good approximation depend only on the overall orientation of the involved peptide plane relative to the magnetic field direction and thereby to the lipid bilayers. Consequently, multi-dimensional NMR experiments of oriented proteins will display unique resonance patterns depending on the peptide secondary structure and its conformation in the membrane. The use of such topology-aided structure elucidation has recently been demonstrated for uniformly ^{15}N-labelled α-helical peptides [80, 81] which lead to characteristic circular resonance patterns – the so-called polarization index slant angle (PISA) wheels – in 2D ^{1}H–^{15}N dipolar coupling/^{15}N shift (PISEMA) correlation experiments [82]. Obviously, the PISA wheels are not unique for the interactions involved in 2D PISEMA experiments as recently illustrated for 2D ^{1}H/^{15}N chemical-shift correlation experiments [83] and a variety of different 2D double- and triple-resonance experiments [84].

A key feature of SIMMOL is its ability to associate different atoms in protein structures (*e.g.*, structures downloaded from the protein database [85] or synthetic structures created using SIMMOL or programs such as WHAT IF [86]) with typical parameters for the magnitude and orientation of anisotropic nuclear spin interaction tensors. This makes SIMMOL an extremely powerful tool for simulation of biological solid-state NMR experiments, such as those described above, on real structures. The SIMMOL output setting up the correct magnitude and *Euler* angles for all specified interactions may be directed to the spin-system part of the SIMPSON input file and subsequently used in a SIMPSON simulation taking into account all ideal/non-ideal features of the NMR experiment as demonstrated elsewhere [31, 32, 84]. However, for fast simulation of PISA wheels we may also choose to disregard the effects from finite pulses and calculate the multiple-dimensional resonance frequencies for the different residues directly in SIMMOL [31]. To do this we use the Tcl output from the SIMMOL commands assigning tensorial

interactions to specific atoms, e.g., `mshift <buffer1>` which specifies chemical shift tensors for the atoms previously assigned to buffer 1 or `mdipole <buffer1> <buffer2> <max> <min>` which identifies all dipole-dipole couplings between atoms in buffer 1 and 2 in the range from `max` to `min`, specified as frequencies or distances. These commands return the atom numbers (from the PDB file) of the involved atoms, the magnitude for the interaction (*e.g.*, δ_{iso}, δ_{aniso}, and η), and the *Euler* angles (Ω_{PL}) describing the orientation of the tensor relative to the laboratory frame.

With the magnetic field oriented along z in the laboratory frame (L), the resonance frequency for an anisotropic interaction may be calculated by transferring the description of the tensor from its principal axis system (P) to L by the transformation

$$A_{\text{L}} = R(\Omega_{\text{PL}})A_{\text{P}}R(\Omega_{\text{PL}})^{T} \tag{4}$$

with A_{P} and $R(\{\Omega\}_{\text{PL}})$ denoting the diagonal principal axis system tensor and the Cartesian rotation matrix. The resonance frequency corresponding to any first-order Hamiltonian [4] is given by the zz element of the A_{L} tensor. We have implemented this coordinate transformation in a Tcl procedure `zzlab <a_p> <angles>`, which uses the SIMMOL Tcl commands `mgeteulermatrix` and `mmath` [31] to manipulate the matrices.

For calculation of PISA wheels, we may use a SIMMOL-synthesized peptide with torsion angles corresponding to ideal α-helix ($\phi = -65°$, $\psi = -40°$), β-strand ($\phi = -135°$, $\psi = 140°$), or any other values of interest and rotate this to form a given tilt angle relative to the magnetic field z axis. Equipped with these structures, SIMMOL allows easy generation of PISA wheels by calculating the resonance frequencies as described above for small increments of the rotational pitch of the peptide. Figure 4 contains four examples of resonance wheel patterns obtained for ideal α-helices tilted differently with respect to the magnetic field and corresponding to a variety of 2D and 3D ^{1}H–^{15}N dipolar coupling, ^{15}N shift, and ^{13}C′ shift correlation experiments. The particular experiments in Fig. 4 are chosen since they have recently been highlighted as particularly relevant for large proteins since they have very attractive properties with respect to resolution power and assignment feasibility [84].

With these simulations we have demonstrated the versatility of SIMMOL for assigning orientation-dependent nuclear spin interactions to polypeptide structures and, with proper Tcl procedures, directly simulate multi-dimensional NMR experiments for uniaxially oriented polypeptides.

SIMPSON and SIMMOL: Optimization of Homonuclear Hartmann-Hahn Polarization Transfer in Liquid-State NMR

The need for reliable and flexible spectral simulations is by no means restricted to solid-state NMR. Although many of the liquid-state applications are performed with standard parameters or are optimized automatically these days, a robust simulation and optimization tool comes in handy when taking even a small step away form the well-paved main road.

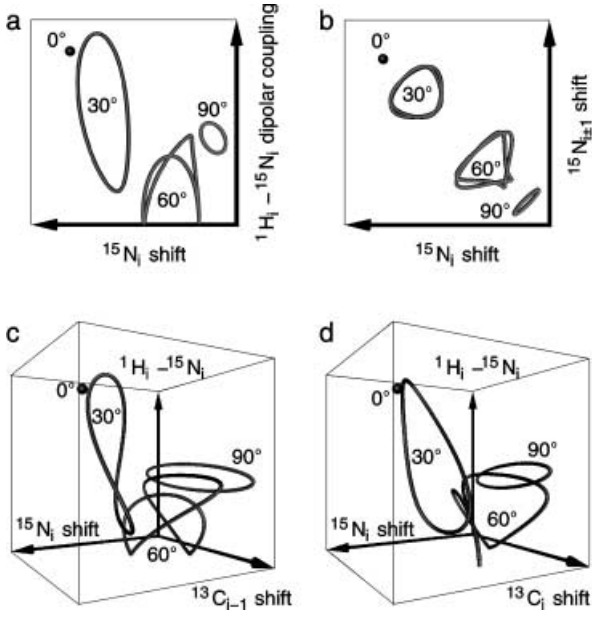

Fig. 4. SIMMOL simulated 2D (a, b) and 3D (c, d) PISA wheels for an ideal α-helix ($\phi = -65°$, $\psi = -40°$) structure with tilt angles of 0°, 30°, 60°, and 90° relative to the magnetic field direction. The simulations represent (a) $^{1}H_i$–$^{15}N_i$ dipolar coupling/$^{15}N_i$ shift (PISEMA), (b) $^{15}N_i/^{15}N_{i\pm1}$ shift, (c) $^{1}H_i$–$^{15}N_i$ dipolar coupling/$^{15}N_i$ shift/$^{13}C'_{i-1}$ shift, and $^{1}H_i$–$^{15}N_i$ dipolar coupling/$^{15}N_i$ shift/$^{13}C'_i$ shift correlation experiments. The displayed frequency ranges (with the arrows pointing from lower to higher frequency) are 0–10 kHz for the ^{1}H–^{15}N dipolar coupling dimension, 50–250 ppm for ^{15}N shift dimensions, and 75–250 ppm for the $^{13}C'$ shift dimensions

An example of parameters that may deserve some attention is that associated with *Hartmann-Hahn* polarization transfer, either it is used for non-selective or selective, homo- or hetero-nuclear transfer. Specifically, we will here look at the possibilities for homonuclear transfer of polarization from the C^{α} to the outermost aliphatic carbon (C^{β} or C^{γ}) in Asx or Glx residues (asparagine and aspartic acid, or glutamine and glutamic acid) at 18.8 T with maximal transfer amplitudes. For the purpose of illustration, we examine the transfer efficiency of DIPSI-2 [87] as function of the rf field strength ($\omega_{\mathrm{rf}}/2\pi$), the mixing time ($\tau_{\mathrm{mix}}$), and the carrier frequency ($\omega_{\mathrm{offset}}/2\pi$).

The low dimensionality of the problem makes it amenable to manual optimization using grid plots as illustrated in Fig. 5. Alternatively, it is straightforward to perform a real optimization using SIMPSON and MINUIT as described in the previous section. Two-dimensional contour plots were calculated for the amplitudes of Asx $C^{\alpha} \rightarrow C^{\beta}$ and Glx $C^{\alpha} \rightarrow C^{\gamma}$ transfer as a function of τ_{mix} and $\omega_{\mathrm{offset}}/2\pi$ at a constant rf field strength of 10 kHz (Fig. 5a–b). Figure 5a shows that the Asx $C^{\alpha} \rightarrow C^{\beta}$ transfer agrees with the expected transfer for a two spin system, *i.e.*, optimal transfer at $\tau_{\mathrm{mix}} = 1/(2J_{\mathrm{CC}})$, $3/(2J_{\mathrm{CC}})$, *etc.* when the carrier is placed in the middle of the spectrum. Although the transfer path is twice as long for Glx, the optimal τ_{mix} values are not much higher ($\sim 1.5/(2J_{\mathrm{CC}})$, $\sim 3.4/(2J_{\mathrm{CC}})$) implying that it should be possible to optimize the Asx and Glx transfers simultaneously. It is

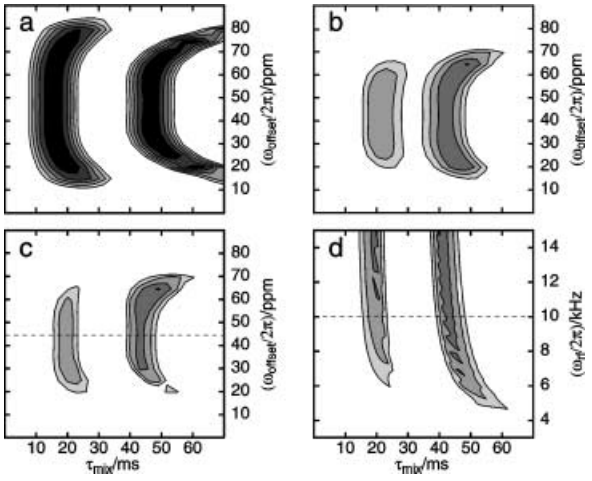

Fig. 5. SIMPSON simulated contour plots of (a) Asx $C^{\alpha} \rightarrow C^{\beta}$ polarization transfer, (b) Glx $C^{\alpha} \rightarrow C^{\gamma}$ transfer, and (c) min{Asx $C^{\alpha} \rightarrow C^{\beta}$, Glx $C^{\alpha} \rightarrow C^{\gamma}$} as a function of τ_{mix} and $\omega_{offset}/2\pi$ at $\omega_{rf}/2\pi = 10$ kHz, and (d) min{Asx $C^{\alpha} \rightarrow C^{\beta}$, Glx $C^{\alpha} \rightarrow C^{\gamma}$} as a function of τ_{mix} and $\omega_{rf}/2\pi$ at $\omega_{offset}/2\pi = 45$ ppm from TMS as indicated by a dashed line in (c). Likewise the rf field strength of 10 kHz employed in (a–c) is shown by a dashed line in (d). The contour levels mark 50% to 90% transfer efficiency in 10% steps, filled with increasingly dark gray. The shift parameters used in these simulations are for Asx: $\delta(C^{\alpha}) = 55$ ppm, $\delta(C^{\beta}) = 40$ ppm, $J_{CC} = 35$ Hz; and for Glx: $\delta(C^{\alpha}) = 55$ ppm, $\delta(C^{\beta}) = 30$ ppm, $\delta(C^{\gamma}) = 35$ ppm. $J_{CC} = 35$ Hz in all cases [88, 89]

interesting to note, that the Glx $C^{\alpha} \rightarrow C^{\gamma}$ transfer tends to increase when the carrier is placed in the region above $\delta(C^{\alpha})$.

To search for optimal sensitivity, contour plots where at each point the smallest of the two transfer amplitudes (min{Asx $C^{\alpha} \rightarrow C^{\beta}$, Glx $C^{\alpha} \rightarrow C^{\gamma}$}) was plotted as a function of τ_{mix} and $\omega_{offset}/2\pi$ at constant $\omega_{rf}/2\pi$ (Fig. 5c), and as a function of τ_{mix} and $\omega_{rf}/2\pi$ at constant $\omega_{offset}/2\pi$ (Fig. 5d) were calculated. These plots show that a transfer of at least 60% for both residue types can be obtained at $\tau_{mix} = 24$ ms ($\sim 1.7/2J_{CC}$) and $\omega_{rf}/2\pi = 7.3$ kHz and 70% at $\tau_{mix} = 21$ ms ($\sim 1.5/2J_{CC}$) and $\omega_{rf}/2\pi = 11$ kHz. If τ_{mix} is increased to 48 ms, a further gain in sensitivity can be achieved, or $\omega_{rf}/2\pi$ can be reduced. However, these gains will compete with losses due to relaxation effects. These were left out for simplicity and will indeed be the limiting factor for larger molecules.

When the backbone carbonyl (C′) and sidechain carbonyls and carboxylates (C^{γ} and C^{δ} for Asx and Glx, respectively) are included in the simulations (not shown) we observe that the maximum efficiency for the desired transfer to the outermost *aliphatic* carbon decreases slightly when the either the rf field strength or the carrier offset are increased. However, the contour plots are virtually identical to those presented in Fig. 5.

SIMPSON and SIMMOL: Visualization of the Spin Evolution During Pulse Sequences

With todays large magnetic field strengths, the bandwidth of normal square pulses of reasonable power may in many cases be too small to cover the whole spectrum of interest. For example, a ^{13}C spectrum spans about 40 kHz at 18.8 T. Thus, it is of

great interest to construct pulses that behave uniformly over this frequency range. *Pines* and co-workers [90, 91] demonstrated that pulses with hyperbolic secant (HS) phase shifts had nice broadband inversion properties, an observation that has later been pursued by several other groups [92–94]. Recently, *Shaka* and co-workers [95] described the use of composite HS pulses for broadband excitation. In particular they demonstrated how three consecutive HS pulses, $\mathrm{HS90}^{\circ}_{x}(\tau) - \mathrm{HS180}^{\circ}_{y}(\tau) - (\tau/2 + \varepsilon) - \mathrm{HS180}^{\circ}_{y}(\tau/2)$, may compensate the unfortunate phase and rf field inhomogeneity behavior of a single 90° HS pulse.

While it is generally accepted that the performance of complicated pulses may exceed that of the standard rectangular pulses, it is much more difficult to visualize and evaluate these pulses and their impact on the spin evolution. In this section we will demonstrate that SIMPSON and SIMMOL through their flexibility allow such analysis to be performed without too much effort. For this purpose, we analyze the HS pulses of *Shaka* and co-workers [95] using the following functionality for the phase and amplitude of the pulses

$$\phi(t) = \phi(0) + \phi_0 \ln\left\{\cosh\left(\frac{10.6t}{\tau}\right)\right\} \tag{5}$$

$$\omega_{\mathrm{rf}}(t) = \omega_{\mathrm{rf}}^{\max}/\cosh\left(\frac{10.6t}{\tau}\right) \tag{6}$$

with $\phi_0 = \pi f_{\max}\tau/10.6$. τ and $f_{\max}$ represent the duration and the band width of the pulse. The three pulse shapes relevant for the composite HS pulse is visualized in Fig. 6a.

These rf schemes may straightforwardly be implemented into SIMPSON at the Tcl scripting level (*i.e.*, in the standard input file) by defining a new procedure `hspulse <tau> <wrfmax> <phase>` with a similar structure as the SIMPSON built-in procedure `pulse <tau> <wrf> <phase>`, *i.e.*,

```
proc hspulse {tau wrfmax phase} {
  set fmax 38e3   # Band width
  set dt   2.0    # Time increment
  set steps [expr int(round($tau/$dt/2))]
  set phi0 [expr 180.0*$fmax*$tau/10.6e6]

  for {set i -$steps} {$i < $steps} {incr i} {
    set x [expr cosh(10.6*$dt*$i/$tau)]
    set phi [expr $phase + $phi0*log($x)]
    set rf [expr $wrfmax/$x]
    pulse $dt $rf $phi
  }
}
```

which allows the three HS pulse sequence ($\tau = 4$ ms, $\varepsilon = 1.8\,\mu$s, and $\omega_{\mathrm{rf}}^{\max}/2\pi$ values of 1.88, 5.64, and 8.41 kHz) to be implemented as

```
hspulse 4000 1880 0
hspulse 4000 5460 90
delay   2001.8
hspulse 2000 8410 90
```

in a SIMPSON input file.

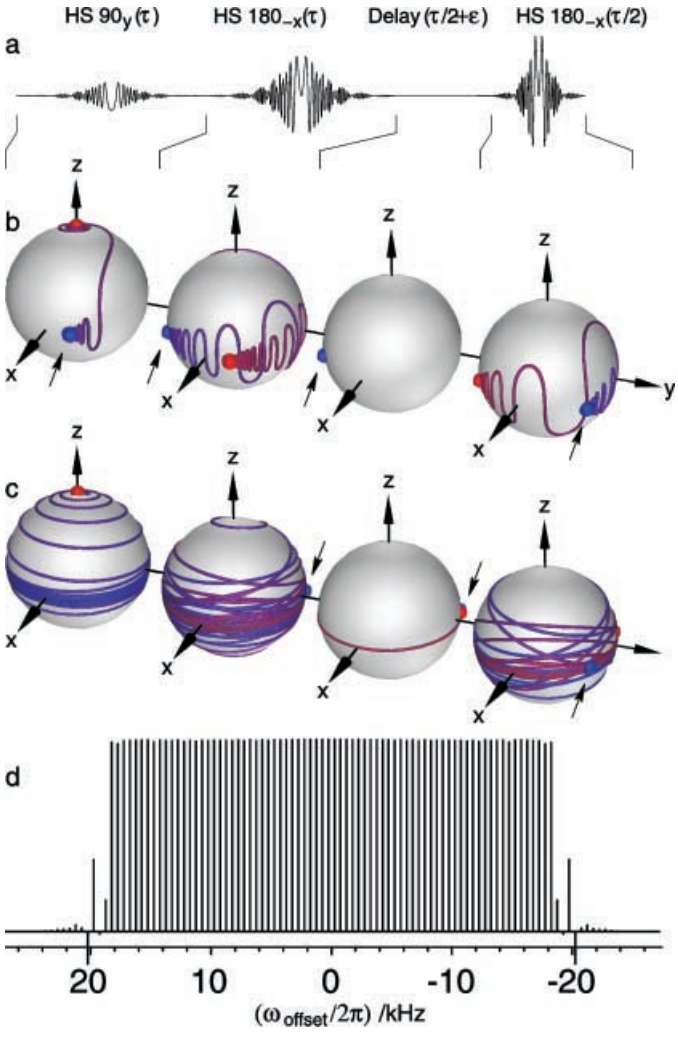

Fig. 6. Pulse-shape (a) employing a train of three hyperbolic pulses employed for broadband excitation [95] (see text). The SIMPSON simulated magnetization trajectories are shown in (b, c) for on-resonance pulses (b) or pulses with an offset of 15 kHz (c). Starting and ending points for the pulse sequence elements are highlighted by small spheres, and in addition the latter points are marked by small arrows. The band width of the pulse is set to $f_{\max} = 38$ kHz. (d) Excitation profile as a function of $\omega_{\text{offset}}/2\pi$ for the pulse sequence in (a)

As a first illustration of the broadbandedness of the composite HS pulse Fig. 6d shows the offset dependence of the pulse as depicted by acquiring the excitation profile ($I_z \rightarrow I_-$) with different transmitter carrier offsets. This simulation employs the above parameters and corresponds to the sum of two experiments with all phases changed in order to achieve a symmetric excitation profile. Indeed, a band width approximately corresponding to $f_{\max}$ is achieved with a very uniform intensity. We note that the simulation in Fig. 6d compares favorably with the experimental result shown in Fig. 7 of Ref. [95].

To gain further insight in the magnetization trajectory during the composite pulse, we have performed a simulation where each of the spin operators I_x, I_y, and

I_z is acquired during the pulse. In SIMPSON this may be done by adding the commands

```
matrix set detect operator I1x
acq
matrix set detect operator I1y
acq
matrix set detect operator I1z
acq
```

in the loop of the `hspulse` procedure. Equipped with these three components, the magnetization trajectory may readily be visualized using any 3D visualization software. To illustrate the versatility of our tools, we have used the ''non-molecular'' visualization functions of SIMMOL (cylinders, arrows, and spheres) to create the images of the magnetization trajectories for on-resonance (Fig. 6b) and 15 kHz-off-resonance (Fig. 6c) pulses. In these figures the large spheres represent the unit sphere on which the magnetization vector travels when neglecting relaxation. The starting- and ending-points of each pulse sequence element are represented by small balls, and in addition the ending point is highlighted by a small arrow. The dark lines on the unit spheres show the magnetization excursions during the pulse sequence elements. We note that both the on-resonance and 15 kHz-off-resonance simulations indeed perform 90° rotations with a *xy* phase independent on the transmitter carrier offset in agreement with the reported properties of these composite pulses [95].

Conclusion

In conclusion, we have through a broad range of different NMR applications demonstrated that the flexibility of SIMPSON and SIMMOL – as provided through the Tcl user interfaces – allows for simulation of essentially all kinds of NMR experiments (disregarding effects from relaxation). This applies for direct simulation of NMR spectra as well as visualization and analysis of the inner working of complex pulse sequences. Besides demonstrating the versatility of SIMPSON and SIMMOL, the various examples have also been selected to add new and powerful features to these programs for the benefit of the users [35]. Beyond any discussion there is a tremendous, and steadily increasing, need for numerical simulations and software of this kind in modern NMR spectroscopy.

Methods

SIMPSON [30] and SIMMOL [31] are open source software packages freely available for download from our web site http://nmr.imsb.au.dk. For 3D visualization of SIMMOL output, we recommend the OOGL (Object Oriented Graphics Language) interpreter Geomview [96]. All simulations have been performed on a 1.9 GHz Pentium IV workstation operating under Linux. The procedures and input files described in this paper can be downloaded from our web site [35].

Acknowledgments

This research was supported by grants from Carlsbergfondet, the Danish Research Agency in relation to the Danish Biotechnology Instrument Centre (DABIC), the Danish Natural Science Research Council, and Novo Nordisk Fonden.

References

[1] Ernst RR, Bodenhausen G, Wokaun A (1987) Principles of Nuclear Magnetic Resonanced in One and Two Dimensions. Calendron Press, Oxford
[2] Wütrich K (1986) NMR of Proteins and Nucleic Acids. Wiley, NY
[3] Cavanagh J, Fairbrother WJ, Parmer III AG, Skelton NJ (1996) Protein NMR Spectroscopy. Principles and Practice. Academic Press, San Diego
[4] Haeberlen U, Waugh JS (1968) Phys Rev **175**: 453
[5] Hohwy M, Nielsen NC (1998) J Chem Phys **108**: 3780
[6] Untidt TS, Nielsen NC (2002) Phys Rev E **65**: 021108-1
[7] Sørensen OW, Eich GW, Levitt MH, Bodenhausen G, Ernst RR (1983) Progr Nucl Magn Reson Spectrosc **16**: 163
[8] Wokaun A, Ernst RR (1977) J Chem Phys **67**: 1752
[9] Vega S (1978) J Chem Phys **68**: 5518
[10] Haeberlen U (1976) High-Resolution NMR in Solids. Selective Averaging. Academic Press, NY
[11] Mehring M (1983) High-resolution NMR in solids. Springer, Berlin, Heidelberg, New York, Tokyo
[12] Spiess HW (1978) Rotations of Molecular and Nuclear Spin Relaxation, NMR Basic Principles and Progress. vol 15, Springer, Berlin
[13] Gerstein BC, Dybowski CR (1985) Transient Techniques in NMR of Solids. An Introduction to Theory and Practice. Academic Press, Orlando
[14] Schmidt-Rohr K, Spiess HW (1996) Multidimensional Solid-State NMR and Polymers. Academic Press, London
[15] Raleigh DP, Levitt MH, Griffin RG (1988) Chem Phys Lett **146**: 71
[16] Gullion T, Schaefer J (1989) J Magn Reson **81**: 196
[17] Gregory DM, Mitchell DJ, Stringer JA, Kiihne S, Shiels JC, Callahan J, Mehta MA, Drobny GP (1995) Chem Phys Lett **246**: 654
[18] Bennett AE, Ok JH, Griffin RG, Vega S (1992) J Chem Phys **96**: 8624
[19] Nielsen NC, Bildsøe H, Jakobsen HJ, Levitt MH (1994) J Chem Phys **101**: 1805
[20] Sommer W, Gottwald J, Demco DE, Spiess HW (1995) J Magn Reson A **113**: 131
[21] Lee YK, Kurur ND, Helmle M, Johannessen OG, Nielsen NC, Levitt MH (1995) Chem Phys Lett **242**: 304
[22] Bielecki A, Kolbert AC, Levitt MH (1989) Chem Phys Lett **155**: 341
[23] Hohwy M, Nielsen NC (1997) J Chem Phys **106**: 7571
[24] Larsen FH, Jakobsen HJ, Ellis PD, Nielsen NC (1998) Mol Phys **95**: 1185
[25] Hohwy M, Jakobsen HJ, Edén M, Levitt MH, Nielsen NC (1998) J Chem Phys **108**: 2686
[26] Verel R, Ernst M, Meier BH (2001) J Magn Reson **150**: 81
[27] Vosegaard T, Florian P, Massiot D, Grandinetti PJ (2001) J Chem Phys **114**: 4618
[28] Opella SJ (1997) Nature Struct Biol **4**: 845
[29] Griffin RG (1998) Nature Struct Biol **5**: 508
[30] Bak M, Rasmussen JT, Nielsen NC (2000) J Magn Reson **147**: 296. SIMPSON is open-source software freely available from the web site http://nmr.imsb.au.dk
[31] Bak M, Schultz R, Vosegaard T, Nielsen NC (2002) J Magn Reson **154**: 28. SIMMOL is open-source software freely available from the web site http://nmr.imsb.au.dk

[32] Bak M, Schultz R, Nielsen NC (2001) In: Kiihne SR, de Groot HJM (eds) Perspectives on Solid State NMR in Biology. Kluwer Academic Publishers, Dordrecht, pp 95–109
[33] Welch BB (1995) Practical Programming in Tcl and Tk. Prentice Hall, Englewood cliffs, NJ. The open source Tcl/Tk software can be downloaded via, eg, the Tcl Developers Xhange homepage, http://dev.scriptics.com
[34] James F, Ross M (1975) Comput Phys Commun **10**: 343. Manual available from the web site http://wwwinfo.cern.ch/asdoc/minuit/minmain.html
[35] The SIMPSON and SIMMOL input files for all examples presented in this paper are available for download from the web site http://nmr.imsb.au.dk. SIMPSON and SIMMOL is open source software freely available from the the same web site
[36] Levitt MH (1989) J Magn Reson **82**: 427
[37] Skibsted J, Nielsen NC, Bildsøe H, Jakobsen HJ (1991) J Magn Reson **95**: 88
[38] Charpentier T, Fermon C, Virlet J (1998) J Magn Reson **132**: 181
[39] Levitt MH, Edén M (1998) Mol Phys **95**: 879
[40] Hohwy M, Bildsøe H, Jakobsen HJ, Nielsen NC (1999) J Magn Reson **136**: 6
[41] Zaremba SK (1966) Ann Mat Pura Appl **4–73**: 293
[42] Conroy H (1967) J Chem Phys **47**: 5307
[43] Cheng VB, Suzukawa Jr HH, Wolfsberg M (1973) J Chem Phys **59**: 3992
[44] Wang D, Hanson GR (1995) J Magn Reson A **117**: 1
[45] Alderman DW, Solum MS, Grant DM (1986) J Chem Phys **84**: 3717
[46] Bak M, Nielsen NC (1997) J Magn Reson **125**: 132
[47] Edén M, Levitt MH (1998) J Magn Reson **132**: 220
[48] Kundla E, Samoson A, Lippmaa E (1981) Chem Phys Lett **83**: 229
[49] Charpentier T, Fermon C, Virlet J (1998) J Chem Phys **109**: 3116
[50] Vosegaard T, Skibsted J, Bildsøe H, Jakobsen HJ (1995) J Phys Chem **99**: 10731
[51] Vosegaard T, Skibsted J, Bildsøe H, Jakobsen HJ (1996) J Magn Reson A **122**: 111
[52] Frydman L, Harwood JS (1995) J Am Chem Soc **117**: 5367
[53] Medek A, Harwood JS, Frydman L (1995) J Am Chem Soc **117**: 12779
[54] Marinelli L, Frydman L (1997) Chem Phys Lett **275**: 188
[55] Marinelli L, Medek A, Frydman L (1998) J Magn Reson **132**: 88
[56] Ding S, McDowell CA (1998) J Magn Reson **135**: 1998
[57] Wu G, Rovnyak D, Griffin RG (1996) J Am Chem Soc **118**: 9326
[58] Madhu PK, Goldbourt A, Frydman L, Vega S (1999) Chem Phys Lett **307**: 41
[59] Madhu PK, Goldbourt A, Frydman L, Vega S (2000) J Chem Phys **112**: 2377
[60] Madhu PK, Levitt MH (2002) J Magn Reson **155**: 150
[61] Kentgens APM, Verhagen R (1999) Chem Phys Lett **300**: 435
[62] Vosegaard T, Larsen FH, Jakobsen HJ, Ellis PD, Nielsen NC (1997) J Am Chem Soc **119**: 9055
[63] Larsen FH, Nielsen NC (1999) J Phys Chem A **103**: 10825
[64] Massiot D (1996) J Magn Reson A **122**: 240
[65] Amoureux JP, Pruski M, Lang DP, Fernandez C (1998) J Magn Reson **131**: 170
[66] Goldbourt A, Madhu PK, Kababya S, Vega S (2000) Solid State Nucl Magn Reson **18**: 1
[67] Vega S, Naor Y (1981) J Chem Phys **75**: 75
[68] Nielsen NC, Bildsøe H, Jakobsen HJ (1992) Chem Phys Lett **191**: 205
[69] Dirken PJ, Nachtegaal GH, Kentgens APM (1995) Solid State Nucl Magn Reson **5**: 189
[70] Amoureux J-P, Fernandez C (1998) Solid State Nucl Magn Reson **10**: 211
[71] Oas TG, Griffin RG, Levitt MH (1988) J Chem Phys **89**: 692
[72] Levitt MH, Oas TG, Griffin RG (1988) Isr J Chem **28**: 271
[73] Gan Z, Grandinetti P (2002) Chem Phys Lett **352**: 252
[74] Walls JD, Lim KH, Pines A (2002) J Chem Phys **116**: 79
[75] Nielsen NC, Vosegaard T, Lipton AS, Ellis PD, unpublished results

[76] Vosegaard T, Massiot D, Grandinetti PJ (2000) Chem Phys Lett **326**: 454
[77] Kunath G, Losso P, Steuernagel S, Schneider H, Jäger C (1992) Solid-State Nucl Magn Reson **1**: 261
[78] Opella SJ, Stewart PL, Valentine KG (1987) Quart Rev Biophys **19**: 7
[79] Cross TA, Quine JR (2000) Concepts Magn Reson **12**: 55
[80] Marassi FM, Opella SJ (2000) J Magn Reson **144**: 150
[81] Wang J, Denny J, Tian C, Kim S, Mo Y, Kovacs F, Song Z, Nishimura K, Gan Z, Fu R, Quine JR, Cross TA (2000) J Magn Reson **144**: 162
[82] Wu CH, Ramamoorthy A, Opella SJ (1994) J Magn Reson A **109**: 270
[83] Marassi FM (2001) Biophys J **80**: 994
[84] Vosegaard T, Nielsen NC (2002) J Biomol NMR **22**: 225
[85] Berstein FC, Koetzle TF, Williams GJB, Meier Jr EF, Brice MD, Rodgers JR, Kennard O, Shimanouchi T, Tasumi M (1977) J Mol Biol **112**: 535 Internet address: http://www.rcsb.org/pdb
[86] Vriend G (1990) J Mol Graph **8**: 52
[87] Shaka AJ, Lee CN, Pines A (1988) J Magn Reson **77**: 274
[88] Sattler M, Schleucher J, Griesinger C (1999) Progr NMR Spectrosc **34**: 93
[89] Schwarzinger S, Kroon GJA, Foss TR, Wright PE, Dyson HJ (2000) J Biomol NMR **18**: 43
[90] Baum J, Tycko R, Pines A (1983) J Chem Phys **79**: 4643
[91] Baum J, Tycko R, Pines A (1985) Phys Rev A **32**: 3435
[92] Bendall MR (1995) J Magn Reson A **112**: 126
[93] Kupche E, Freeman R (1996) J Magn Reson A **118**: 299
[94] Tannús A, Garwood M (1996) J Magn Reson A **120**: 133
[95] Cano KE, Smith MA, Shaka AJ (2002) J Magn Reson **155**: 131
[96] Levy S, Munzner T, Philips M et al (1996) Geomview 1.6.1, University of Minesota, Minneapolis. Geomview is open source software freely available from the web site http://www.geomview.org